IVYSPRING INTERNATIONAL PUBLISHER

Theranostics

2016; 6(2): 272-286. doi: 10.7150/thno.13350

Research Paper

In vivo MR and Fluorescence Dual-modality Imaging of Atherosclerosis Characteristics in Mice Using Profilin-1 Targeted Magnetic Nanoparticles

Yabin Wang[1, 2#], Jiangwei Chen[2#], Bo Yang[1#], Hongyu Qiao[2], Lei Gao[1], Tao Su[2], Sai Ma[2], Xiaotian Zhang[2], Xiujuan Li[2], Gang Liu[3], Jianbo Cao[3], Xiaoyuan Chen[4], Yundai Chen[1✉], Feng Cao[1, 2✉]

1. Department of Cardiology, Chinese PLA General Hospital, Beijing, 100853, China
2. Department of Cardiology, Xijing Hospital, Fourth Military Medical University, Shaanxi, 710032, China
3. Center for Molecular Imaging and Translational Medicine, Xiamen University, Xiamen, 361005, China
4. Laboratory of Molecular Imaging and Nanomedicine (LOMIN), National Institute of Biomedical Imaging and Bioengineering (NIBIB), National Institutes of Health (NIH), Bethesda, MD 20892-2281, USA

Contribute equally to this work

✉ Corresponding authors: Feng Cao, Department of Cardiology, Chinese PLA General Hospital, Beijing, 100853, China. E-mail:wind8828@gmail.com. Co-corresponding to Yundai Chen, cyundai@126.com.

Received: 2015.07.27; Accepted: 2015.10.29; Published: 2016.01.01

Abstract

Aims: This study aims to explore non-invasive imaging of atherosclerotic plaque through magnetic resonance imaging (MRI) and near-infrared fluorescence (NIRF) by using profilin-1 targeted magnetic iron oxide nanoparticles (PF_1-Cy5.5-DMSA-Fe_3O_4-NPs, denoted as PC-NPs) as multi-modality molecular imaging probe in murine model of atherosclerosis. **Methods and Results:** PC-NPs were constructed by conjugating polyclonal profilin-1 antibody and NHS-Cy5.5 fluorescent dye to the surface of DMSA-Fe_3O_4-nanoparticles *via* condensation reaction. Murine atherosclerosis model was induced in apoE$^{-/-}$ mice by high fat and cholesterol diet (HFD) for 16 weeks. The plaque areas in aortic artery were detected with Oil Red O staining. Immunofluorescent staining and Western blot analysis were applied respectively to investigate profilin-1 expression. CCK-8 assay and transwell migration experiment were performed to detect vascular smooth muscle cells (VSMCs) proliferation. *In vivo* MRI and NIRF imaging of atherosclerotic plaque were carried out before and 36 h after intravenous injection of PC-NPs. Oil Red O staining showed that the plaque area was significantly increased in HFD group ($p<0.05$). Immunofluorescence staining revealed that profilin-1 protein was highly abundant within plaque in HFD group and co-localized with α-smooth muscle actin. Profilin-1 siRNA intervention could inhibit VSMCs proliferation and migration elicited by ox-LDL ($p<0.05$). *In vivo* MRI and NIRF imaging revealed that PC-NPs accumulated in atherosclerotic plaque of carotid artery. There was a good correlation between the signals of MRI and *ex vivo* fluorescence intensities of NIRF imaging in animals with PC-NPs injection. **Conclusion:** PC-NPs is a promising dual modality imaging probe, which may improve molecular diagnosis of plaque characteristics and evaluation of pharmaceutical interventions for atherosclerosis.

Key words: Atherosclerosis, Profilin-1, DMSA-Fe_3O_4-nanoparticles, Molecular imaging

Introduction

Atherosclerosis and its cardiovascular complications are the leading causes of morbidity and mortality worldwide. Most of the major cardiovascular diseases may be ascribed to rupture of vulnerable atherosclerotic plaque and secondary thrombosis formation [1, 2]. Occurrence of vulnerable plaque is a

complicated biological process, including endothelial dysfunction, macrophage infiltration, inflammatory factors expression, intra-plaque neovascularization, intima-media remodeling and so on [3]. How to dynamically monitor changes of biomarkers for vulnerable plaque remains a crucial problem.

Molecular imaging, which can non-invasively monitor development of lesions on cellular and protein levels, enables more accurate diagnosis of atherosclerotic plaque [4, 5]. It is also able to provide more comprehensive and dynamic evaluation of therapeutic efficacy for diseases. It has been reported that elastin-targeted MRI contrast agent (BMS-753951) is capable of noninvasively detecting plaque development and vascular remodeling, identifying in-stent restenosis in pig coronary arteries [6]. Although novel noninvasive molecular imaging for atherosclerotic plaque has been under development, accurate assessment of plaque characteristics and vulnerability is still in its infancy. It is necessary to further enhance the sensitivity and specificity of molecular imaging for atherosclerosis.

Acquiring more specific biomarkers aimed at different composition of plaque is critical to the construction of multimodal molecular imaging platform. Profilin-1, a type of small actin-binding protein, is involved in the modulation of cytoskeleton polymerization and reorganization. Recent research shows that profilin-1 overexpression triggers the occurrence and development of cardiovascular diseases such as atherosclerosis, hypertension and cardiac hypertrophy, mainly through regulating vascular smooth muscle cells (VSMCs) proliferation and migration [7-9]. Therefore, profilin-1 is recognized as a promising potential molecular target of atherosclerosis, which may reflect VSMCs features under pathological conditions. To date, there is hardly any molecular probe targeted at activated VSMCs in plaque.

In the present study, we aimed to utilize profilin-1 as molecular target, apply DMSA-Fe_3O_4 nanoparticles as probe carrier to targeted profilin-1 for multimodality MRI/NIRF imaging. We further evaluated the ability of profilin-1-Cy5.5-DMSA-Fe_3O_4-NPs (PC-NPs) to target VSMCs *in vitro* and to assess atherosclerotic plaque characteristics after atorvastatin administration in mice atherosclerotic model through MRI and NIRF imaging *in vivo*.

Materials and Methods

Study design

12-week-old male apoE$^{-/-}$ mice (Jax West Laboratories, West Sacramento, CA, USA) were first fed standard laboratory chow diet for one week. Thereafter, all animals were randomly allocated into three groups with n=20 each, (1) Control group: mice kept on a standard laboratory chow diet (TD.88137, Harlan Laboratories Inc., Madison, WI) for 16 weeks; (2) High fat and cholesterol diet (HFD) group: mice were fed with a western type diet (containing 15% fat and 0.25% cholesterol) for 16 weeks; (3) HFD+Atorvastatin group: mice were fed with a western type diet and atorvastatin (5 mg/kg body weight/day by oral gavage) for 16 weeks. All animal procedures were conducted in conformity with the National Institutes of Health Guideline on the Use of Laboratory Animals and all experiments were performed in accordance with the Helsinki declaration.

Synthesis of Fe_3O_4-DMSA nanoparticles

To prepare for Fe_3O_4 nanoparticles firstly, iron (III) chloride ($FeCl_3 \cdot 6H_2O$)(1.0 mol·L^{-1}) and $FeSO_4 \cdot 7H_2O$ (0.5 mol·L^{-1}) were firstly diluted in 100 ml of deionized water in a three-neck flask, followed by adding concentrated $NH_3 \cdot H_2O$ solution with stirring at 70°C under a nitrogen atmosphere until a pH of 11.0. The temperature was kept at 70°C and the reaction was continued for 5min, and Fe_3O_4 nanoparticles were acquired. After that, Oleic acid (OA, 6 ml) was slowly added to the reaction solution. After 30min of reaction, the temperature was raised to 85°C for 1 h, and then cooled down to room temperature. Black precipitates were collected by magnetic separation and carefully washed with deionized water and ethanol several times. The obtained Fe_3O_4-OA nanoparticles were dissolved in 100 ml of hexane. Fe_3O_4-OA (240mg) and meso-2,3-Dimercaptosuccinic acid (DMSA, 120 mg) were dissolved in 120 ml of mixed solution of acetone and hexane (volume ratio of 1:1) with stirring at 60°C for 4 h. Then DMSA-Fe_3O_4 nanoparticles were collected by magnetic separation and washed with deionized water several times, and then dissolved in 20 ml of deionized water.

Characterization of Fe_3O_4-DMSA nanoparticles

DMSA-Fe_3O_4 nanoparticles were firstly prepared in PBS buffer. The iron oxide core size of DMSA-Fe_3O_4 nanoparticles was measured by transmission electronmicroscopy (TEM, JEM-200CX, JEOL, Japan). The average hydrodynamicparticle size and zeta potential (ζ) values of the nanoparticles were characterized using a Zetasizer Nano ZS (Malvern Instruments, Worcestershire, UK) equipped with a 4 mW He-Ne laser (λ = 633 nm) at room temperatures ranging from 22℃ to 27℃. The magnetic properties of the samples were performed by a vibrating sample magnetometer (VSM, Model LS7400, Lakeshore, USA) with a maximum applied field of 10,000 Oe at room temperature.

Serum lipid profiles analysis

The serum was separated after blood sample coagulation. Then, serum levels of triglycerides (TG), total cholesterol (TC), low-density lipoprotein cholesterol (LDL-C) and high-densitylipoprotein cholesterol (HDL-C) were detected by ELISA using automatic biochemical processer.

Tissue collection and morphological analysis

After euthanasia, the total length of carotid artery and descending aorta was taken out entirely, opened longitudinally with the intima towards the outside. Then, tissues were stained in pre-warmed Oil Red O solution for 10 min and differentiated in 85% propylene glycol for 5 min at room temperature (RT). To further assess the atherosclerotic plaque, mice carotid artery and descending aorta were removed and frozen in Optimum Cutting Temperature (OCT) compound. Consecutive frozen aortic sections (10 μm thickness) were prepared and stained with Oil Red O for 10 min, followed by counterstaining with hematoxylin for 1-3 min at RT. Image J software was used to quantify the lesion areas of the entire vascular intima.

Immunofluorescence staining

Atherosclerotic tissues obtained from mice carotid artery and descending aorta were prepared as 5 μm thick serial OCT embedded cryosections. The frozen sections were immersion-fixed in 4℃ acetone for 20 min, washed in PBS three times, and blocked with 2% BSA at RT for 45 min. Thereafter, the sections were incubated separately with rabbit anti-mouse profilin-1 antibody (1:200, Abcam, Cambridge, UK), goat anti-mouse α-smooth muscle actin (α-SMA) antibody (1:200, Abcam, Cambridge, UK) overnight at 4℃, followed by incubation with TRITC rabbit anti-goat IgG (1:200; Abcam, Cambridge, UK) and FITC goat anti-rabbit IgG (1:200; Santa Cruz Biotechnology, CA, USA) secondary antibodies for 1 h at 37°C in a humidified box. Then, the sections were washed in PBS three times and counterstained with DAPI (1:1000; BioworldBiotechnology, Minnesota, USA). Tissue slides were visualized with a confocal microscopy (Olympus FV10i, Tokyo, Japan).

Western blot analysis

Tissue protein samples and cells samples were extracted from the aorta of mice and *in vitro* VSMCs respectively. The protein were subjected to 10% SDS-PAGE and transferred to nitrocellulose (NC) membranes (Millipore, Billerica, MA, USA) using a semi-dry electroblotting system. After blocking with 5% skim milk in PBS, the membranes were incubated with diluted polyclonal rabbit anti-mouse profilin-1 (1:1000) and a monoclonal anti-β-actin antibody (1:1000, Abcam, Cambridge, UK) at 4°C overnight. After washing and further incubation with appropriate secondary antibodies conjugated with horseradish peroxidase (dilution: 1:5000 in TBST) at 37°C for 60 min, bands were visualized using an enhanced chemiluminescence system (ECL; Amersham). Densitometry analysis of Western blots was carried out using VisionWorks LS, version 6.7.1(Caliper Life Sciences, Hopkinton, USA).

Smooth muscle cell culture

The mouse aorta smooth muscle cell line (MOVAS) was purchased from American Type Culture Collection (ATCC) center (Menassas, VA, USA). MOVAS were cultured in Dulbecco's Modified Eagle Medium (DMEM) (Sigma-Aldrich, USA), containing 1% penicillin–streptomycin and 10% fetal bovine serum (FBS) (Sigma-Aldrich, USA).Cells were incubated in humidified 5% CO_2, 37 °C incubator (Thermo, MA, USA) and measured by a hemocytometer. Cells were co-stained by alpha-SMA (Abcam, Cambridge, UK) and DAPI (Bioworld Biotechnology, Minnesota, USA), and imaged with an Olympus BX51 fluorescent microscope (Olympus, Tokyo, Japan).

The siRNA targeting of profilin-1 siRNA transfection

Profilin-1 siRNA and control siRNA were purchased commercially from Genechemistry (Shanghai, China). The sequence of the mouse profilin-1siRNA (5′ to 3′) was as follows (RNA): 5′-CGTTACGGACGC GGCCATCG-3′; 5′-CAGCGTGCGTGATGTTGACG A-3′. Control siRNA: 5′-TTC AAG UCC UCG ACG ACU UUG-3′; 5′-CTC AAA GUC GUC CAG CAG UUG-3′. MOVAS were seeded onto 60-mm dishes 24 h before transfection and then transiently transfected with 100 nM Profilin-1siRNA or control siRNA per dish at 90% confluence using the lipofectamine 2000 (Invitrogen Life Technology, USA) according to the manufacturer's protocol. Successful knockdown of the target proteins was confirmed by Western blot analysis.

Cell viability assay

The cell viability of MOVAS was detected by using cell counting kit-8 (CCK-8, Beyotime institute of biotechnology, Jiangsu province, China). Cells were seeded in 96-well plates (2000 cells/well) and incubated with fresh medium at a 37°C and 5% CO_2 atmosphere for 24h. Then, the fresh medium was replaced by fresh medium containing ox-LDL (20μg/ml) or profilin-1 siRNA. After 48h, cells were washed with PBS for 3 times and incubated in 100 μl DMEM (Sigma-Aldrich, St. Louis, MO) containing 10 μl CCK-8 solution for 2h. The absorbance at 450nm

was measured by using ELISA reader. The fresh medium without cells was served as blank controls respectively. Following subtracting the blank cell OD_{450}, the treated cell proliferation rate was calculated as a percentage of the absorbance to control cell absorbance.

Transwell migration assay

The effects of ox-LDL on MOVAS migration were investigated by a transwell migration chamber (8.0 μm; Millipore, Billerica, MA, USA). 1.0×10^5 cells were seeded in upper chamber of transwell insert containing serum-free cell culture medium (400 μl). The same medium with ox-LDL (20 μg/ml) as a chemoattractant was added to the lower chamber. The chamber was cultured at 37°C in 5% CO_2 humidified atmosphere for 4 h. Non-migrating cells on the upper surface of chamber were wiped out and washed with phosphate-buffered saline (PBS). The rest of the cells were fixed in 4% paraformaldehyde and then stained by crystal violet solution (Beyotime Institute of Biotechnology, Beijing, China). The cells were counted under a microscope at per five independent HPF (×200).

In vitro cytotoxicity assay

To assess cytotoxicity of DMSA-Fe_3O_4 nanoparticles, MOVAS and RAW 264.7 cells were seeded on a 96-well plate at 70% confluence, and then various concentrations of Fe_3O_4 nanoparticles and DMSA-Fe_3O_4 nanoparticles were separately added into different wells, followed by incubation for 24 h at 37°C in 5% CO_2 humidified atmosphere. MTT assay was performed to estimate the number of viable cells after nanoparticles' treatment.

Construct profilin-1-Cy5.5-DMSA-Fe_3O_4 nanoparticles (PC-NPs) and IgG-1-Cy5.5-DMSA-Fe_3O_4 nanoparticles (IC-NPs)

Polyclonal profilin-1 antibody was conjugated to DMSA-Fe_3O_4 nanoparticles at room temperature as described before. Firstly, pH of the reaction system (Fe_3O_4-DMSA nanoparticles solution) was adjusted to 6.0, 7.0, 8.0, 9.0 using different doses of boric acid/borate buffer (0.02 M, pH=9.0) respectively. Then, EDC (0.01 ml, 10 mg/ml) and sulfo-NHS (0.005 ml, 10 mg/ml) were dissolved in DMSA-Fe_3O_4 nanoparticles solution (1.0ml, 1.0mg/ml) and stirred for 15 min at RT. Then, 50 μg of profilin-1 antibody (0.1mg/ml, pH 7.4) was added into the solution. After stirring for another 4 h at RT, the compounds were centrifuged (15,000 × *g*, 30 min) to remove the uncoupled monoclonal antibody. The profilin-1 antibody was successfully conjugated with Fe_3O_4-DMSA nanoparticles, which was confirmed by UV (ultraviolet)-Vis absorption spectroscopy (Shimadzu, Kyoto, Japan). The conjugation efficiency was calculated by measuring the ratio of labeled proteins to DMSA-Fe_3O_4 nanoparticles concentration using acid (BCA) Protein Assay (Beyotime Institute of Biotechnology, Beijing, China). Cy5.5-NHS (GE Healthcare, USA) was combined to react with PF_1 labeled DMSA- Fe_3O_4 nanoparticles in a 3:1 dye to protein molar for 2 h at RT with shaking. Unconjugated dye was removed by size exclusion chromatography on a 10DG desalting column (Bio-Rad, California, USA) as described previously[10](Scheme 1). IC-NPs were constructed by conjugating IgG antibody to the surface of DMSA-Fe_3O_4 nanoparticles, and other steps were the same as mentioned above.

Biodistribution of PC-NPs

To investigate tissue biodistribution of PC-NPs *in vivo*, probe at a dose of 2 mg/kg Fe was intravenously injected into apoE$^{-/-}$ mice from the tail vein. At 12, 24, 36 hour post-injection, mice were euthanized and major organs, i.e. liver, lung, kidney, heart, bone, muscle, were collected for fluorescent imaging analysis *ex vivo* under the IVUS Imaging System (Xenogen Imaging Technologies, Alameda, CA), using the following parameters: exposure time (10s), f/stop (2), binning (4), and field of view (12.8).

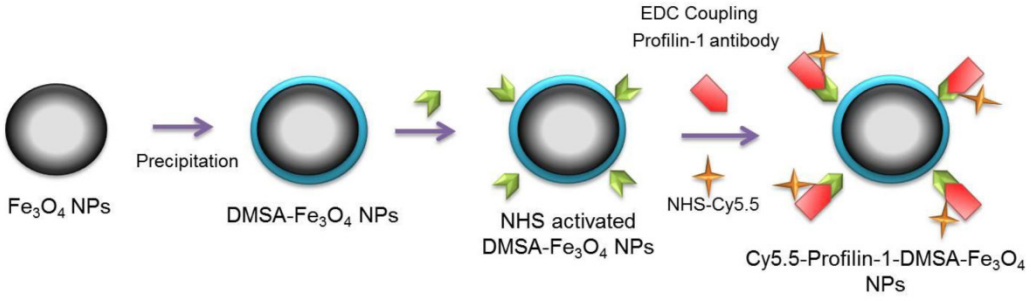

Scheme 1. Schematic diagram of profiling-1-Cy5.5-DMSA- Fe_3O_4 nanoparticles

MR imaging with PC-NPs *in vivo*

ApoE$^{-/-}$ mice were anesthetized with 1.5% isoflurane and underwent MR imaging of the carotid arteries using a 9.4 T small animal MRI system (BrukerBiospec, Billerica, MA, USA) with 30mm birdcage coil. T_2-weighted MRI was operated before and at 24, 36 and 48 hour post-administration of PC-NPs at a dose of 2mg/kg Fe using the following 3D Flash (Fast low-angle shot) sequence parameters: repetition time [TR]/echo time [TE] =14.7/4.6 ms; flip =30°; field of view=2.5 cm × 2.5 cm; matrix=256 × 256, slice thickness=0.5 mm. MR images were analyzed using OsiriX image analysis software. The aortic wall was identified and signal intensities of regions of interest (ROI) were obtained with a custom-made Matlab (MathWorks, Natick, MA), and were analyzed by two observers who were blinded to histopathological data. Contrast to noise ratio (CNR) of each ROI was calculated as the average signal intensity divided by the standard deviation of the noise level. Relative enhancement ratios with respect to the average CNR ($CNR_{changes}$) were calculated and plotted as a percentage decrease in CNR over the time by the following formula: $\%CNR_{changes} = (CNR_{post}-CNR_{pre}) / CNR_{pre}\times100\%$. CNR_{pre} was obtained from images before PC-NPs administration, while CNR_{post} represents SNRs calculated from images acquired 36 h after injection.

Fluorescence imaging with PC-NPs *in vivo* and *ex vivo*

Fluorescence imaging was acquired after intravenous injection of PC-NPs at a dose of 2mg/kg Fe (IVIS Lumina XR system (Caliper Life Sciences, Hopkinton, USA), using the following parameters: exposure time (60s), f/stop (2), binning (4), and field of view (12.8). Then, Fluorescence imaging was continuously observed for the following three days. After final *in vivo* fluorescence imaging, the animals were euthanized, and the carotid arteries and aorta of animals were carefully excised and washed with saline three times. Then quantification of *in vivo* and *ex vivo* NIRF signal intensities of entire carotid arteries were analyzed as previous method[11] with Living Image version 4.4 software (Caliper Life Sciences, Hopkinton, USA).

Immunohistochemistry analysis

Sections obtained from the carotid arteries were stained with hematoxylin and eosin for morphometric analysis. Perl's blue staining was applied to identify the probe deposit. All images were reviewed under light microscope and Perl's positive cells were counted by a blinded manner.

After Cy5.5 fluorescence imaging *ex vivo* performed, the carotid tissues were snap frozen in liquid nitrogen and stored at -70℃. Aixal sections (10μm thickness) acquired were prepared for immunofluorescent staining of smooth muscle cells marker α-SMA. All images were reviewed under confocal laser scanning microscope (Olympus, Tokyo, Japan) by a blinded manner.

Statistical analysis

All values are expressed as means±SEM. Results were analyzed by1-sample t test versus 100, unpaired Student t tests, or for multiple comparisons ANOVA and the Student–Newman–Keulspost test. A least squares method and a linear regression model are used to analyze the correlation between MR signals and fluorescence imaging data. Significant differences were accepted when $p<0.05$.

Results

Serum lipid profile

After being fed with standard laboratory chow or western type diet, there was no significant difference in body weight of all groups. Compared with the control group, LDL-C and TC levels were significantly increased in the HFD group (LDL-C: 12.56 ± 0.73 mM *vs.* 2.08 ± 0.08 mM, $p < 0.05$; TC: 26.47 ± 0.75 mM *vs.* 2.40 ± 0.32 mM, $p < 0.05$). Administration of atorvastatin reversed serum LDL-C and TC levels ($p<0.05$). In addition, serum level of HDL-C was decreased in HFD group, in contrast to control group (HDL-C: 0.84 ± 0.05 mmol/L *vs.* 1.44 ± 0.03 mmol/L, $p<0.01$). However, atorvastatin did not affect HDL-C level (Figure 1A).

Atherosclerotic plaque formation

Atherosclerotic plaque formation was evaluated by quantitative analysis of the plaque area in the total aorta with Oil O Red staining. The plaque area was significantly increased in HFD group, compared with control group (the ratio of plaque area to whole artery area: 85.33% ± 0.05% in HFD group *vs.* 18.02% ± 0.03% in control group, $p<0.01$). However, atorvastatin significantly decreased atherosclerotic lesions (HFD+Atorvastatin group: 54.05% ± 0.06% *vs.* HFD group: 85.33% ± 0.05%, $p<0.05$). Oil red O-stained frozen cryosections of carotid arteries further verified that the atherosclerotic plaque was attenuated after atorvastatin treatment (Figure 1B).

Profilin-1 is widely expressed in atherosclerosis plaque

Western blot analysis revealed that profilin-1 protein was highly expressed in arterial wall of the HFD group in contrast to that of the control group ($p<0.05$). Nevertheless, atorvastatin treatment mark-

edly reduced profilin-1 expression (p<0.05) (Figure 2A). Moreover, the results of immunofluorescence co-staining further revealed that profilin-1 protein was highly abundant within plaque, compared with control group. Majority of profilin-1 protein was co-localized with α-SMA (VSMCs marker) and there was still some present in extracellular space (Figure 2B).

Profilin-1 silencing inhibits ox-LDL-induced MOVAS proliferation and migration

To further analyze the correlation between profilin-1 expression and MOVAS proliferation as well as migration, CCK-8 and transwell assays were performed. CCK-8 assay results showed that ox-LDL (20μg/ml) induced VSMCs proliferation, which was able to be reversed by profilin-1 siRNA intervention (p<0.05). Likewise, transwell migration analysis revealed that profilin-1 siRNA was also able to abrogate ox-LDL-elicited MOVAS migration (p<0.05) (Figure 3A and 3B). Immunofluorescence analysis revealed that ox-LDL (20 μg/ml) markedly promoted profilin-1 expression in the cytoplasm of MOVAS (p<0.01) (Figure 4A).

Consistent with immunofluorescence results, Western blot analysis also showed ox-LDL promoted profilin-1 expression in MOVAS (p<0.05). In addition, ox-LDL also increased MEK and ERK1/2 phosphorylation (p<0.05). However, profilin-1 siRNA intervention attenuated profilin-1 expression, as well as MEK and ERK1/2 phosphorylation induced by ox-LDL (p<0.05) (Figure 4B).

Characterization of Fe_3O_4-DMSA nanoparticles

To construct profilin-1 targeted molecular imaging probe, DMSA-Fe_3O_4 nanoparticles were first prepared and characterized. The TEM image of DMSA-Fe_3O_4 nanoparticles (DMSA-Fe_3O_4-NPs) is shown in Figure 5A; as mearsured, the nanoparticles display mono-dispersion with average sizes of 7 nm in dry state (Figure 5B). As shown in Figure 5C, the average hydrodynamic size of nanoparticles is 30.2 nm. Moreover, the particles carry a negative zeta potential of - 42.7mv. The hysteresis curves of DMSA-Fe_3O_4-NPs have been portrayed in Figure 5D, and the saturation magnetization value (M_s) is 56.4 emu g^{-1}. In addition, the relativity (r2) of DMSA-MNPs is calculated to be 134.5 $mM^{-1}s^{-1}$ (Figure 5E).

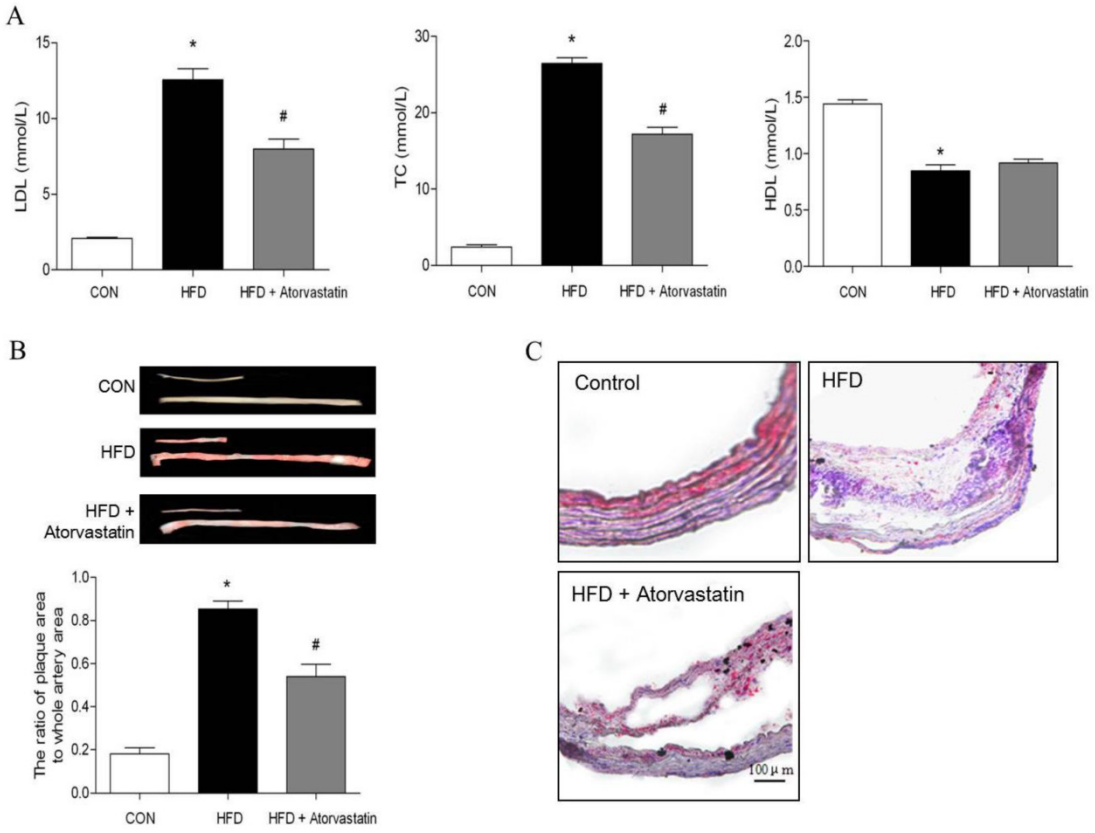

Figure 1. Atorvastatin decreased serum lipid level and atherosclerotic lesion formation induced by high-fat diet in apolipoprotein E-deficient (apoE$^{-/-}$) mice. Serum LDL, total cholesterol and HDL were measured in apoE$^{-/-}$ mice fed on a high-fat diet for 16 weeks. (B) Oil Red O staining of the total length of carotid artery from different mice after 16-week HFD feeding, and subsequently quantitation of mean Oil Red O stained plaque area (n= 5 per group; *p<0.05 *vs.* control group, #p<0.05 *vs.* HFD group). (C) Tissue sections made of the atherosclerotic lesion-prone aortic root were stained for Oil Red O.

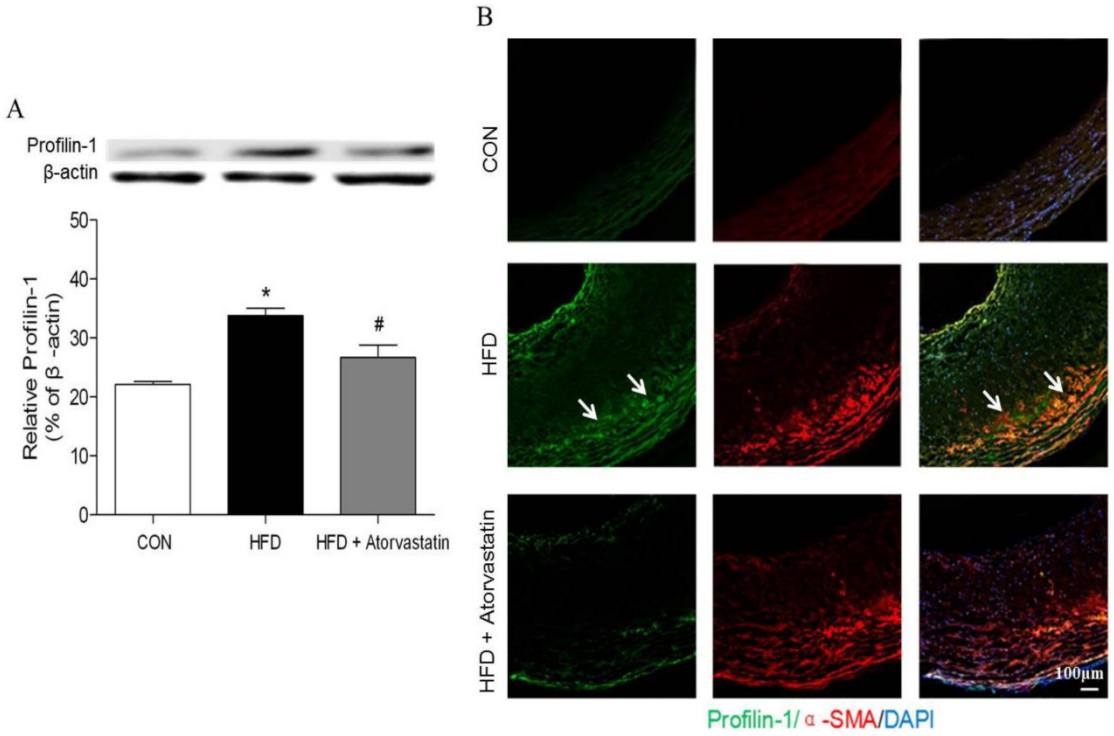

Figure 2. Atorvastatin attenuated profilin-1 expression in atherosclerotic plaque of apoE$^{-/-}$ mice. Western blot analysis was performed to assess profilin-1 expression in plaque (n= 5 per group; *p<0.05 *vs.* control group, #p<0.05 *vs.* HFD group). (B) Confocal microscopy of plaque from aortic vessel wall of apoE$^{-/-}$ mice with profilin-1(green), alpha-smooth muscle actin (alpha-SMA)(red). The nuclei were stained with 4,6-diamino-2-phenylindole (DAPI) (blue). The co-localization of green and red signals appeared as orange colors. Scar bar: 100 μm.

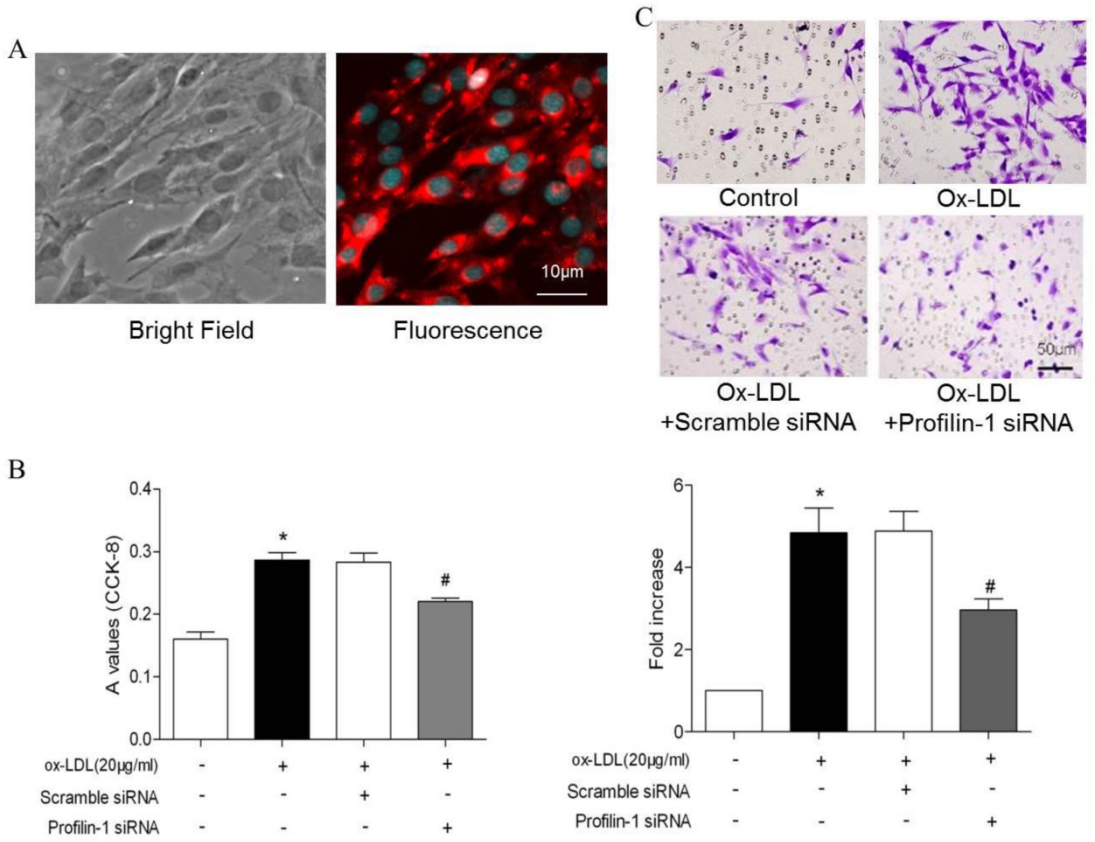

Figure 3. Effect of profilin-1 siRNA on VSMCs proliferation and migration induced by ox-LDL. (A) Morphology and immunofluorescence staining of VSMCs. (B) After 24 hours, VSMCs proliferation was detected by CCK-8 assay (n= 5 per group; *p<0.05 *vs.* control group, #p<0.05 *vs.* ox-LDL group). (C) After 24 hours, VSMCs migration was measured by transwell experiment. Ox-LDL (20μg/ml) was included in the lower chamber as chemo-attractant (n= 5 per group; *p<0.05 *vs.* control group, #p<0.05 *vs.* ox-LDL group).

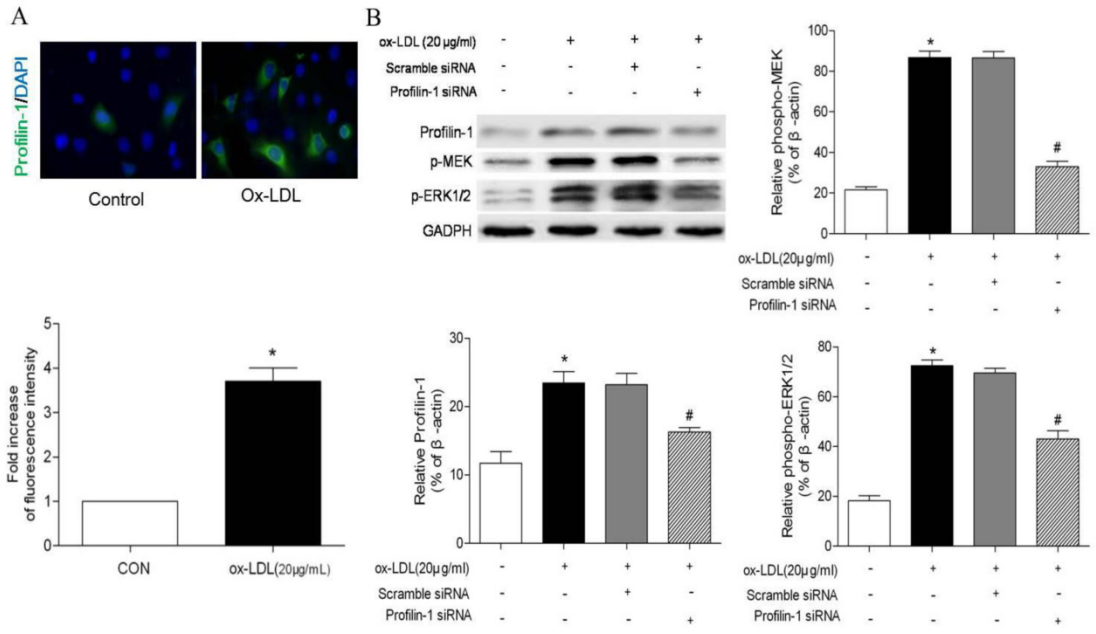

Figure 4. Effect of profilin-1 siRNA on phosphorylation of MEK and ERK1/2 in VSMCs induced by ox-LDL. Profilin-1 expression (green fluorescence) in VSMCs was determined by confocal microscopy. (B) Phosphorylation of MEK and ERK1/2 in VSMCs induced by ox-LDL was evaluated by Western blot assay (n= 5 per group; *p<0.05 *vs.* control group, #p<0.05 *vs.* ox-LDL group).

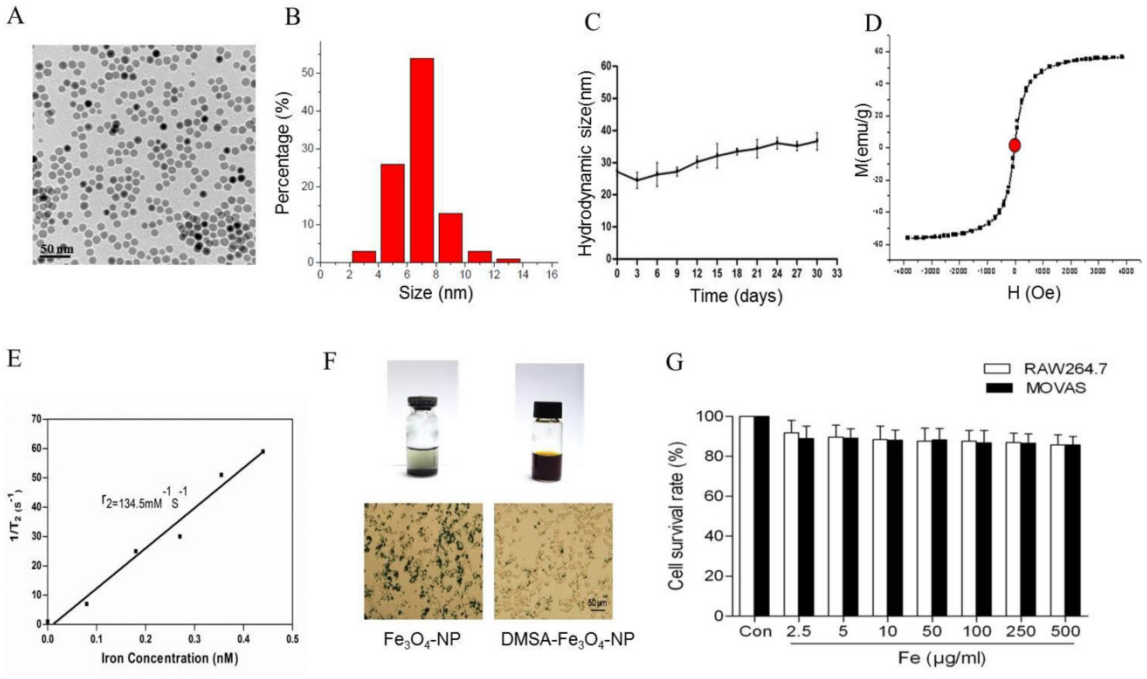

Figure 5. Characterization of DMSA-Fe_3O_4 nanoparticles. TEM demonstrated roughly spherical, monodisperse nanoparticles with a mean diameter of 7 nm. (B) The size distribution of DMSA-Fe_3O_4 nanoparticles was detected by Zetasizer Nano ZS. (C) The magnetic properties of the samples were performed by a vibrating sample magnetometer. (D) The relaxivity (r2) of DMSA-MNPs. (E) Stability and biocompatibility of DMSA-Fe_3O_4 nanoparticles. (F) MOVAS and RAW264.7 cells survival were assessed by MTT assay.

In vitro stability and biocompatibility of DMSA-Fe_3O_4

To detect the stability of DMSA-Fe_3O_4-NPs, we laid nanoparticle solution for two weeks at room temperature. It is observed that there was some precipitation in Fe_3O_4-NPs solution, while none in the DMSA-Fe_3O_4-NPs solution (Figure 5F). Macrophage phagocytosis experiment revealed that much more Fe_3O_4 nanoparticles were phagocytized by macrophages than DMSA-Fe_3O_4-NPs. MTT assay showed that DMSA-Fe_3O_4-NPs exerted no significant effect on vascular smooth muscle cell and macrophage viability exposed up to 24 hours, even at concentrations as high as 0.5 mg/ml (Figure 5G).

Labeling efficiency and *in vivo* tissue distribution of PC-NPs

UV (ultraviolet)-Vis absorption spectroscopy results showed that PC-NPs had an absorption band in the range of 250-300 nm, whereas unlabeled DMSA-Fe_3O_4-NPs did not have (Figure 6A). It suggests that profilin-1 antibody was successfully conjugated with DMSA-Fe_3O_4-NPs. To further measure the average number of profilin-1 antibodies per DMSA-Fe_3O_4-NP, BCA protein assay and orthophenanthroline photometric method were performed respectively to analyze protein and iron content of PF_1-DMSA-Fe_3O_4-NPs. The data reveals that per DMSA-Fe_3O_4-NP is labeled with nine profilin-1 antibody molecules (Figure 6B and 6C).

In order to study the tissue distribution of PC-NPs *in vivo*, NIR fluorescence was performed in normal C57BL/6J mice after intravenous injection of 100 μl PC-NPs (0.04 mg Fe). As shown in Figure 6D, PF_1-DMSA-Fe_3O_4-NPs accumulated mainly in liver and kidneys at 24 h post-injection, while almost cleared from all organs at 48 h post -injection.

Fluorescence imaging of PC-NPs *in vitro*, *in vivo* and *ex vivo*

In vitro fluorescence imaging results showed that the highest cell binding of PC-NPs to MOVAS was observed in MOVAS pretreated with ox-LDL (20μg/ml) for 4h. However, when the MOVAS were co-cultured with unconjugated DMSA-Fe_3O_4-NPs, the binding rate decreased significantly. Likewise, when MOVAS were co-cultured directly with PC-NPs but without ox-LDL pretreatment or with Profilin-1 siRNA intervention, the cell binding rate was also significantly reduced (Figure 7A). In addition, being different from the targeting ability of PC-NPs to VSMCs, it did not exhibit specific binding to ox-LDL pretreated macrophages (Figure 7B).

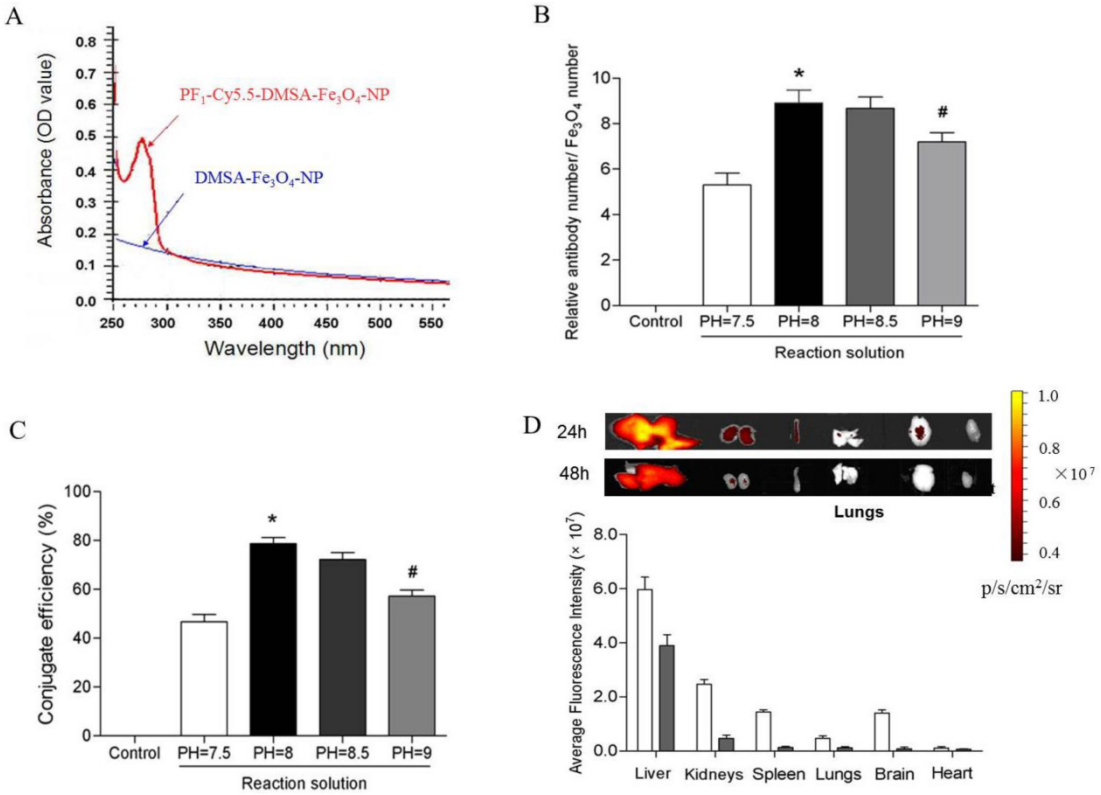

Figure 6. Conjugation efficiency and *in vivo* tissue distribution of profilin-1-Cy5.5-DMSA-Fe_3O_4 nanoparticles. UV (ultraviolet)-Vis absorption spectroscopy analysis of profilin-1-Cy5.5-DMSA-Fe_3O_4 nanoprobe. (B) Relative ratio of profilin-1 antibody to Cy5.5-DMSA-Fe_3O_4 nanoparticles at different reaction solution. (n=3 per group;*p<0.05 *vs.* PH=7.5 reaction solution, #p<0.05 *vs.* PH=8 reaction solution). (C) Conjugate efficiency of profilin-1-Cy5.5-DMSA-Fe_3O_4 nanoparticles at different reaction solution. (D) Fluorescence imaging of *in vivo* tissue distribution of profilin-1-Cy5.5-DMSA-Fe_3O_4 nanoparticles at 24 and 48 h after probe injection.

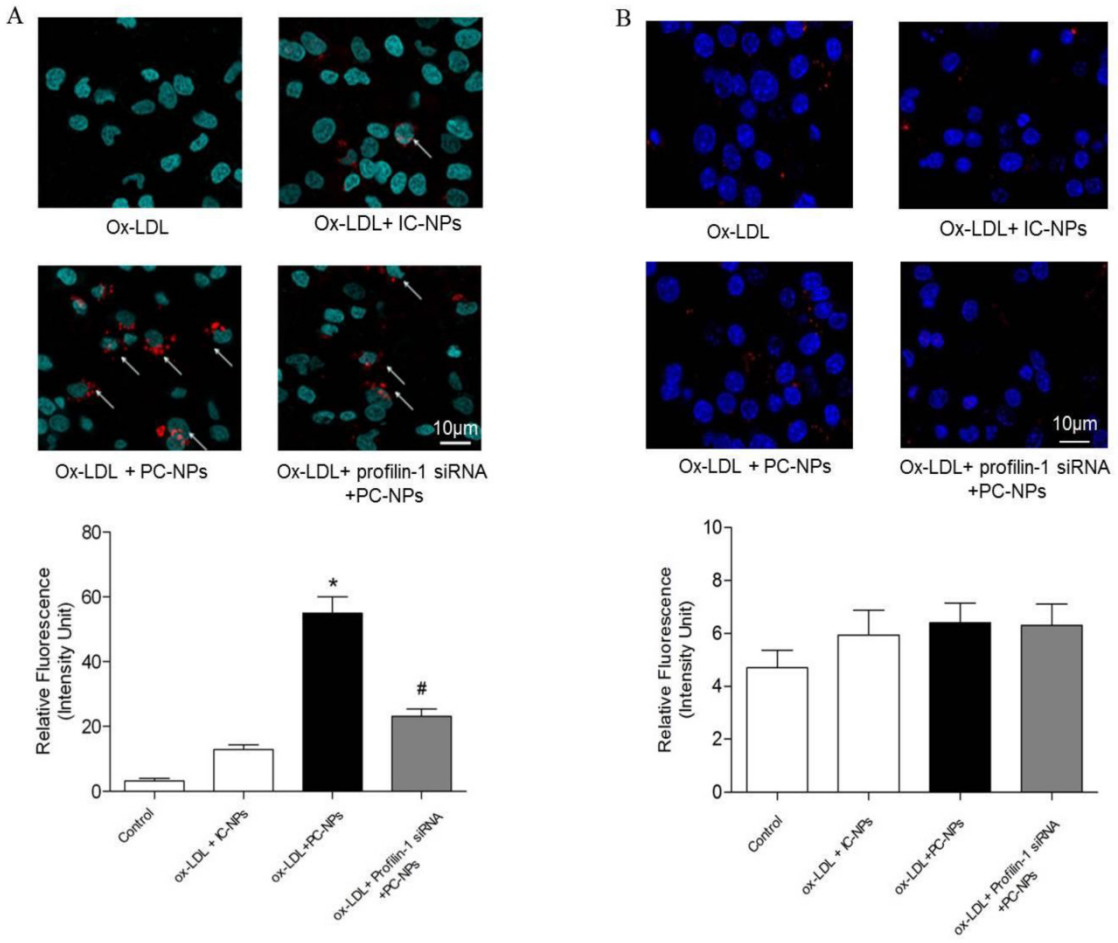

Figure 7. Fluorescence imaging of profilin-1-Cy5.5-DMSA-Fe_3O_4 nanoparticles's binding ability to VSMCs and macrophages *in vitro*. Binding ability of profilin-1-Cy5.5-DMSA-Fe_3O_4 nanoparticles to VSMCs induced by ox-LDL *in vitro*. (n=5 per group; **p*<0.05 *vs.* ox-LDL+Cy5.5-DMSA-Fe_3O_4 nanoparticles, #*p*<0.05 *vs.* ox-LDL + profilin-1 siRNA profilin-1-Cy5.5-DMSA-Fe_3O_4 nanoparticles). (B) Binding ability of profilin-1-Cy5.5-DMSA-Fe_3O_4 nanoparticles to macrophages induced by ox-LDL *in vitro*. (n=5 per group; *p*=NS).

Cy5.5 NIR fluorescence images *in vivo* were acquired 36 h after intravenous injection of PC-NPs or IC-NPs. The results revealed that fluorescence signal at the carotid artery were significantly higher in the HFD + PC-NPs injection group, compared with the HFD + IC-NPs injection group ($p<0.05$). Atorvastatin treatment was able to significantly attenuate fluorescence signal of the carotid artery ($p<0.05$) (Figure 9A). Then Cy5.5 NIR fluorescence imaging was performed again after opening the neck of apoE$^{-/-}$ mice. The results showed significantly higher NIRF signal in the carotid arteries of PF_1-DMSA-Fe_3O_4-NPs group, compared with other groups ($p<0.05$) (Figure 9B). *Ex vivo* NIRF imaging also confirmed this (Figure 9C).

MRI of atherosclerotic plaque with PC-NPs in vivo

To observe atherosclerotic plaque in apoE$^{-/-}$ mice through MRI, *in vivo* 9.4T MR imaging were performed before and 36h after injection of PC-NPs. As revealed in Figure 8A, apoE$^{-/-}$ mice exhibited increased wall thickness and pronounced plaque formation compared to controls. Although there were almost no signal changes in carotid arteries wall on T_2-weighted MRI after administration of IC-NPs, a significant T_2-weighted MRI signal attenuation was observed 36 h post PC-NPs injection in HFD mice group compared with other groups. There was no significant T_2 signal change observed in HFD + Atorvastatin treatment group and IC-NPs injection group.

To analyze signal intensity changes at the carotid artery in a more quantitative way, we defined a contrast to noise ratio (CNR). As shown in Figure 8C, CNR value was attenuated significantly in HFD + PC-NPs injection group, compared to HFD + IC-NPs injection group (31.70% ± 3.21% *vs.* 9.47% ± 0.92%, $p<0.05$). However, atorvastatin treatment abrogated CNR changes in arterial wall post PC-NPs injection. In addition, NIR fluorescence images of PC-NPs *in vivo* exhibited correlations with *in vivo* MRI signal changes ($CNR_{changes}$). The correlation coefficients were 0.9338 (R^2=0.8719) for fluorescence imaging intensity with *in*

vivo $CNR_{changes}$ (Figure 9C). It's notable that *ex vivo* fluorescence images of PC-NPs also have good correlations with *in vivo* MRI signal changes ($CNR_{changes}$) (Figure 9D).

Histology verification

Perl's staining further confirmed that more nanoparticles deposited in atherosclerotic lesions of HFD + PC-NPs injection group than those in other groups (Figure 10A).

Immunofluorescent staining α-SMA of carotid arteries tissue showed that there was better co-localization of PC-NPs with immunofluorescent α-SMA signal, in contrast to other non-targeted probes (Figure 10B).

Discussion

Molecular imaging is a promising technique for the visualization atherosclerosis development and its characteristics non-invasively, which may predict vulnerability of plaque [12]. However, its clinical application is still limited, mainly due to the lack of proper contrast agents with fine biocompatibility and specificity. It is well recognized that acquiring specific biomarkers to construct targeted probe is key to molecular imaging of atherosclerosis. It is reported that actin-binding protein profilin-1 plays important roles in the occurrence and development of cardiovascular diseases including atherosclerosis, hypertension and diabetic complication [7, 8]. In the present study, we observed that profilin-1, an actin-binding protein associated with VSMCs proliferation and migration, was highly expressed in atherosclerotic plaque. Then, we constructed PC-NPs as molecular imaging probe and used it to *in vivo* visualize atherosclerotic plaque in $apoE^{-/-}$ mice through NIR fluorescence and MR imaging. It is likely that increased accumulation of PC-NPs in atherosclerotic lesions led to significant signal changes in T_2-weighted MRI and NIR fluorescence imaging of plaque compared to other non-targeted nano-probes.

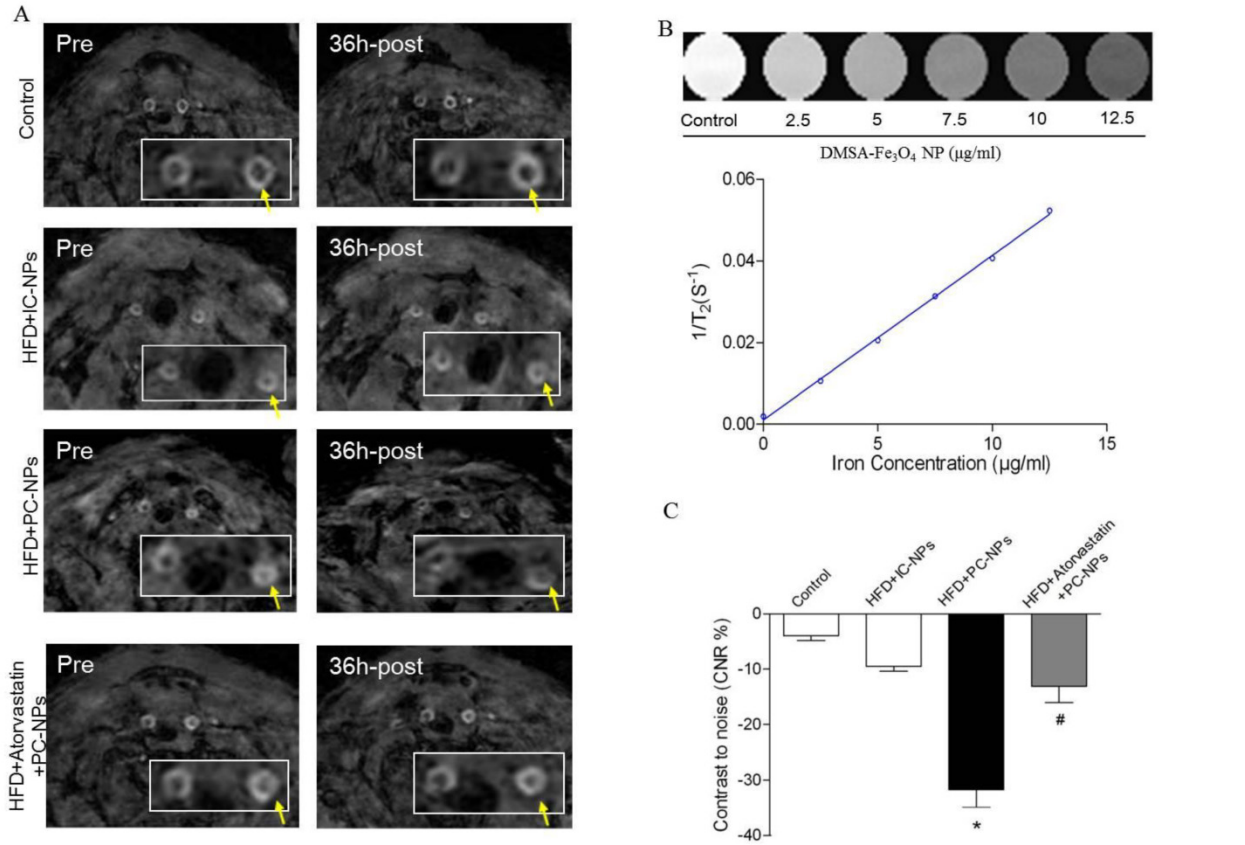

Figure 8. Magnetic Resonance Imaging of $ApoE^{-/-}$ Mice with Profilin-1-Cy5.5-DMSA-Fe_3O_4 nanoparticles *in vivo*. Representative in vivo MR images obtained before and 36 h after administration of profilin-1-Cy5.5-DMSA-Fe_3O_4 nanoparticles in $apoE^{-/-}$ mice. (B) Standard curve generated by quantifying MRI $1/T_2$ value of known concentration of profilin-1-Cy5.5-DMSA-Fe_3O_4 nanoparticles. (C) Quantification analysis of MRI signal changes in carotid artery of $apoE^{-/-}$ mice before and 36 h after administration of profilin-1-Cy5.5-DMSA-Fe_3O_4 nanoparticles. (n=5 per group; $^*p<0.05$ *vs.* HFD + Cy5.5-DMSA-Fe_3O_4 nanoparticles, $^\#p<0.05$ *vs.* HFD + atorvastatin treatment + profilin-1-Cy5.5-DMSA-Fe_3O_4 nanoparticles)

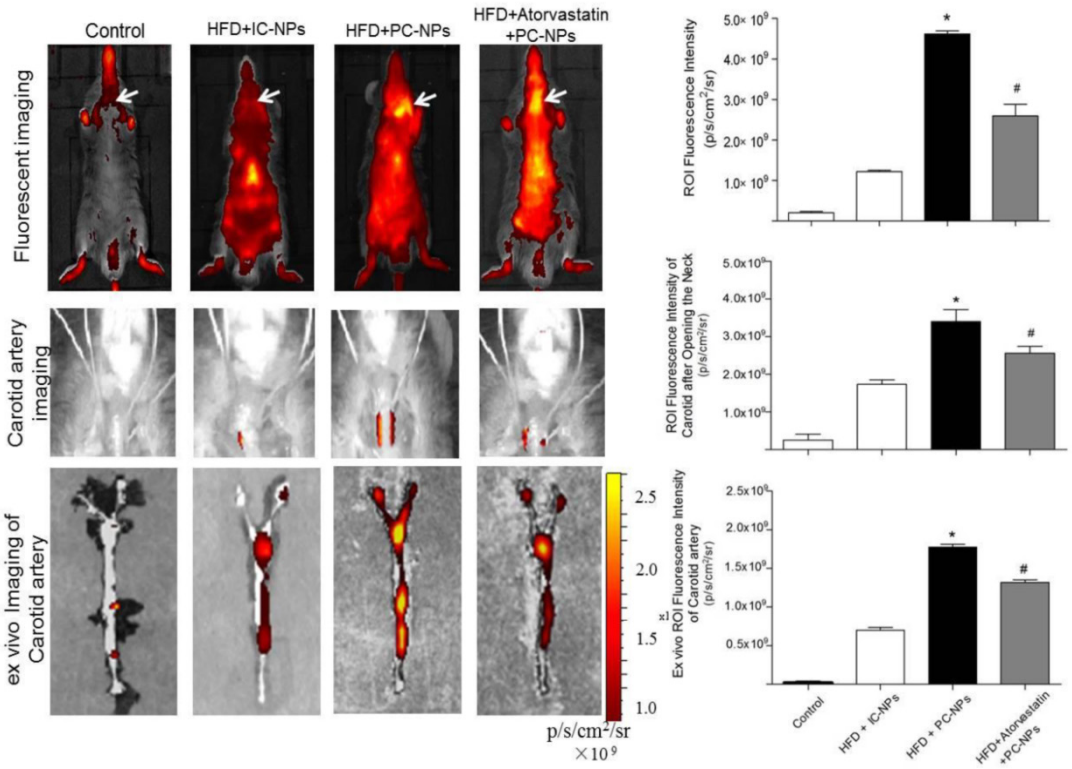

Figure 9. In vivo and ex vivo near-infrared fluorescent imaging of carotid atheromata of apoE$^{-/-}$ mice after the intravenous injection of probes. (A) In vivo fluorescence imaging of apoE$^{-/-}$ mice after intravenous injection of profilin-1-Cy5.5-DMSA-Fe_3O_4 nanoparticles. (n=5 per group; *p<0.05 *vs.* HFD + IgG-Cy5.5-DMSA-Fe_3O_4 nanoparticles, #p<0.05 *vs.* HFD + atorvastatin treatment + profilin-1-Cy5.5-DMSA-Fe_3O_4 nanoparticles). (B) In vivo fluorescence imaging of apoE$^{-/-}$ mice after opening the neck. (n=5 per group; *p<0.05 *vs.* HFD + IgG-Cy5.5-DMSA-Fe_3O_4 nanoparticles, #p<0.05 *vs.* HFD + atorvastatin treatment + profilin-1-Cy5.5-DMSA-Fe_3O_4 nanoparticles). (C) Ex vivo fluorescent imaging confirmed that profilin-1-Cy5.5-DMSA-Fe_3O_4 nanoparticles deposited in carotid artery. (n=5 per group; *p<0.05 *vs.* HFD + IgG-Cy5.5-DMSA-Fe_3O_4 nanoparticles, #p<0.05 *vs.* HFD + atorvastatin treatment + profilin-1-Cy5.5-DMSA-Fe_3O_4 nanoparticles).

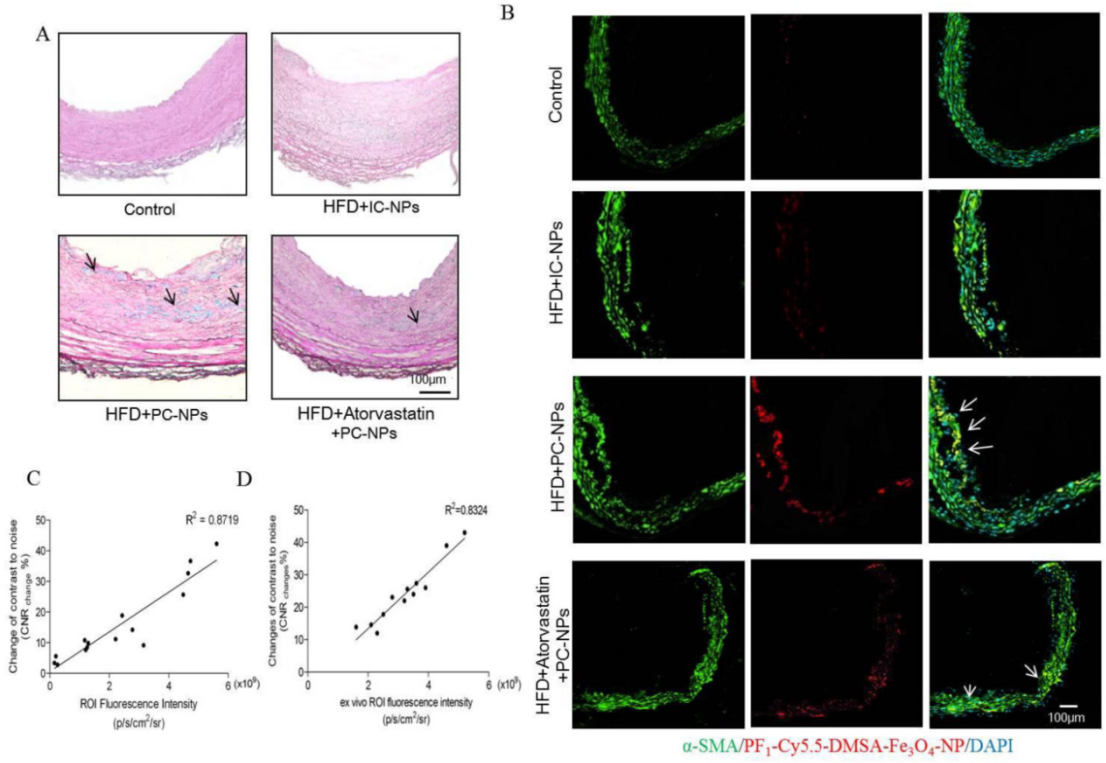

Figure 10. Histology analysis confirmed that profilin-1-Cy5.5-DMSA-Fe_3O_4 nanoparticles deposited in atherosclerotic lesions. (A) Perl's staining confirmed that profilin-1-Cy5.5-DMSA-Fe_3O_4 nanoparticles deposited in atherosclerotic lesions. (B) Confocal immunofluorescence microscophy showed profilin-1-Cy5.5-DMSA-Fe_3O_4 nanoparticles colocalized with VSMCs marker α-SMA. (C) Correlations of MR images with in vivo Fluorescence images obtained 36 h after profilin-1-Cy5.5-DMSA-Fe_3O_4 nanoparticles injection. (D) Correlations of MR images with ex vivo Fluorescence images.

In recent studies, it is well established that profilin-1, an actin-binding protein, plays pivotal roles in cellular functions including proliferation, survival, migration and membrane trafficking [13]. Its overexpression can trigger smooth muscle cell dysfunction, which consequently results in vascular disorders and cardiovascular diseases. On the other hand, the silencing of profilin-1 protein may exert protective roles from pathological conditions (e.g. hypertension, atherosclerosis and diabetes) [14]. In this research, we found that profilin-1 was mainly expressed in vascular smooth muscle cells of atherosclerotic lesions. Then, we exposed VSMCs to ox-LDL for 24 hours in order to elucidate the relationship between VSMC migration and profilin-1 expression. The data illustrated that exposure of VSMCs to ox-LDL contributed to a significant increase in cell proliferation and migration, which was mediated by profilin-1. These results were consistent with previous studies, demonstrating that profilin-1 can serve as a target protein of atherosclerosis [7, 8]. Thus, we chose profilin-1 as a molecular target for visualizing atherosclerotic lesions *in vivo*.

It is necessary to synthesize contrast agent with good biocompatibility and low cytotoxicity for clinical available imaging. Of all non-invasive clinical imaging modalities, MRI is more attractive because of its lack of radiation, and its ability to facilitate deep tissue imaging and to provide high spatial resolution [15, 16]. Ultra-small super-paramagnetic iron oxide nanoparticles (USPIO) were frequently applied as probe carrier in MRI to enhance image contrast in the detection of atherosclerotic plaque [17]. Segers FM *et al* found that scavenger receptor-AI-targeted molecular imaging of USPIO-based contrast agents hold great promise for detection of inflammatory plaques [18]. In present study, we utilized DMSA-Fe_3O_4-NPs, a type of USPIO, as the core of contrast agent. TEM images indicated that DMSA-Fe_3O_4-NPs didn't aggregate during the conjugation process. The data of diameter distribution analysis suggested that the DMSA-Fe_3O_4-NPs belonged to ultra-small nanoparticles, which contributed to the decreased uptake by the reticulo-endothelial system. Cellular uptake experiments also confirmed that phagocytosis of DMSA-Fe_3O_4-NPs by macrophages were less than conventional Fe_3O_4-NPs. The hysteresis curves showed that DMSA-Fe_3O_4-NPs were super paramagnetic material with saturation magnetization of 56.4 emu g^{-1}. Following characterization of NPs, MTT assay indicated that DMSA-Fe_3O_4-NPs exhibited no significant cytotoxicity. Based on these, it can be concluded that synthesized DMSA-Fe_3O_4-NPs with favorable properties such as decreased phagocytosis, increased circulation and the lack of cytotoxity, were suitable for serving as the MRI contrast agent. MRI, however, has its shortcomings of not being able to distinguish well between tissues of similar densities. In contrast, near-infrared fluorescence (NIRF) imaging can overcome those deficiencies, since it includes high-sensitivity, relatively simple operation and inexpensive equipment [19]. Multimodality-based molecular imaging is the future direction for observing the structural and functional alterations of lesions *in vivo*. Therefore, to track progression of atherosclerosis in living subjects with more sensitivity and accuracy, we conjugated fluorescent dye Cy5.5 to DMSA-Fe_3O_4-NPs in order to construct a dual-modality contrast agent. In addition, to further improve the specific target of the contrast agent, profilin-1 antibody was functionalized to the surface of Cy5.5-DMSA-Fe3O4-NPs through a condensation reaction between amino group of profilin-1 antibody and carboxylic acid on surface of IC-NPs. UV-visible absorbance indicated that profilin-1 antibody was successfully conjugated on to the surface of IC-NPs.

In order to image plaque progression and characteristics, we applied atorvastatin treatment in animals, followed by a dynamic monitoring of the atherosclerosis plaque by PC-NPs MR/NIR imaging. Firstly, *in vitro* binding study indicated that PC-NPs exhibited higher specific binding efficiency to ox-LDL-induced MOVAS than nonspecific probe. However, the binding ability of PC-NPs was attenuated in VSMCs after profilin-1 siRNA treatment, which was mainly due to silencing of profilin-1 abrogating proliferation and profilin-1 expression of VSMCs. Then, *in vivo* NIR fluorescence imaging results suggest that PC-NPs showed preferential accumulation at the plaque than non-targeted IC-NPs. Atorvastatin therapy inhibited plaque progression, which contributed to less localization of IC-NPs in lesions. However, *in vivo* Cy5.5 fluorescence signals may not actually come from carotid arteries due to the noise from adjacent anatomical structures (e.g. skin/hair/nerve/vein/fat/muscles/ cartilages). Therefore, in order to figure out the accurate loaction of *in vivo* fluorescence signals, we performed *in vivo* and *ex vivo* NIR fluorescence imaging of carotid arteries after the open-neck surgery on apoE$^{-/-}$ mice. All of these results confirm Cy5.5 fluorescence signals came from carotid arteries. Furthermore, PC-NPs preferentially localized in the plaque of carotid arteries, compared with other non-targeted probes groups.

Furthermore, it is worth to note that MRI emerges as a promising non-invasive method for imaging of atherosclerosis [20], which can provide image of artery vessel wall with excellent spatial resolution, in contrast to fluorescence imaging [21, 22]. In the present study, PC-NPs also can serve as MRI contrast

agent, in addition to NIRF probe. Therefore, localization of targeted PC-NPs in atherosclerotic lesions was further confirmed by MRI of carotid artery of apoE$^{-/-}$ mice. T2-weighted images of 9.4T MRI showed that the signal intensity of carotid artery was significantly attenuated at 36 h post PC-NPs injection, in comparison to probe pre-injection. Wei C et al. reported that HDL nanoparticles labeled with collagen-specific EP3533 peptides could be used to noninvasively visualize intra-plaque macrophages and collagen content in mouse atherosclerotic plaques. The different trends of macrophage and collagen contents were correlated with the changes of in vivo MR signals of aortic walls after the injection of EP3533-HDL contrast agents [23]. This correlation suggests that MR signals in aortic vessel can likely reflect different composition of the plaque. Therefore, we further quantitatively evaluated MRI T2-weighted signal attenuation in carotid artery *in vivo* by calculating contrast to signal ratio (CNR). It is confirmed that there exists a positive correlation between the concentration of DMSA-Fe_3O_4-NPs solution and the degree of signal-attenuation. These data also suggest that PC-NPs exhibited preferential localization to atherosclerotic lesions, which was further confirmed by Perl's staining of carotid artery *ex vivo*. MR and NIR signals alteration after using PC-NPs contrast agent is capable of representing vascular smooth muscle cells content in the atherosclerotic lesion.

Compared with other dual-modality probes (e.g. PS-25 FMT-CT probe, collagen-specific EP3533, VCAM-1-specific ^{99m}Tc-labeled probe)[23-25], our PC-NPs exhibit proper size distribution, ability to penetrate into inflamed plaques, minimal uptake into circulating leukocytes and blood background fluorescence as well as specific targted to activated VSMCs.

Despite of these advantages, our probe has some limitations. For instance, PC-NPs have longer plasma half-time which leads to the delay for ideal imaging time to get maximum plaque signal. Therefore, we should improve PC-NPs's design with faster kinetics property and clinically that is desirable injection-imaging interval time. Secondly, the probe of PC-NPs without anti- atherosclerotic drug or siRNA can only be utilized in the diagnosis of plaque instead of diagnosis and therapy integration. Thirdly, although MR and NIR dual-modality imaging of atherosclerotic lesions can be achieved using PC-NPs contrast agent, image fusion of the same tissue with MRI and NIRF still needs to be studied further.

In summary, we have demonstrated that PC-NPs, profilin-1-targeted probe with favorable biocompatibility, can be used for dual MR and optical imaging of atherosclerotic plaque in mice. Furthermore, this targeted probe is also helpful to evaluate therapeutic efficacy of atherosclerosis dynamically and non-invasively. By combining the imaging of VSMCs with PC-NPs and macrophage with other available probes such as scavenger receptor-AI-targeted iron oxide nanoparticles [18], the characteristics and vulnerability of plaque can be comprehensively assessed *in vivo* during the development of lesions.

Acknowledgements

This work was supported by the National Funds for Distinguished Young Scientists of China (No. 81325009), and National Natural Science Foundation of China (No.81270168, No.81530058, 81570272, 81500360, 81227901, 81570272), Innovation Team Development Grant by China Department of Education (IRT1053), Shaanxi Province Program (2013K12-02-03), Key Science and Technology Innovation Team in Shaanxi Province (No.2014KCT-20), and Beijing Natural Science Foundation (7132227).

Abbreviations

USPIO: super-paramagnetic iron oxide nanoparticles; CNR: contrast to signal ratio; IC-NPs: IgG-Cy5.5-DMSA-Fe_3O_4-NPs; PC-NPs: PF_1-Cy5.5-DMSA-Fe_3O_4-NPs; HFD: High fat and cholesterol diet; VSMCs: vascular smooth muscle cells; MRI: Magnetic Resonance Imaging; NIRF: near-infrared fluorescence.

Competing Interests

The authors have declared that no competing interest exists.

References

[1] Erbel R, Budoff M. Improvement of cardiovascular risk prediction using coronary imaging: subclinical atherosclerosis: the memory of lifetime risk factor exposure. European heart journal. 2012;33:1201-13.
[2] Wang H, Eitzman DT. Acute myocardial infarction leads to acceleration of atherosclerosis. Atherosclerosis. 2013;229:18-22.
[3] Foin N, Evans P, Krams R. Atherosclerosis: cell biology and lipoproteins - new developments in imaging of inflammation of the vulnerable plaque. Current opinion in lipidology. 2008;19:98-100.
[4] Chan JM, Monaco C, Wylezinska-Arridge M, Tremoleda JL, Gibbs RG. Imaging of the vulnerable carotid plaque: biological targeting of inflammation in atherosclerosis using iron oxide particles and MRI. European journal of vascular and endovascular surgery : the official journal of the European Society for Vascular Surgery. 2014;47:462-9.
[5] Wildgruber M, Swirski FK, Zernecke A. Molecular imaging of inflammation in atherosclerosis. Theranostics. 2013;3:865-84.
[6] von Bary C, Makowski M, Preissel A, Keithahn A, Warley A, Spuentrup E, et al. MRI of coronary wall remodeling in a swine model of coronary injury using an elastin-binding contrast agent. Circulation Cardiovascular imaging. 2011;4:147-55.
[7] Romeo GR, Moulton KS, Kazlauskas A. Attenuated expression of profilin-1 confers protection from atherosclerosis in the LDL receptor null mouse. Circulation research. 2007;101:357-67.
[8] Romeo GR, Pae M, Eberle D, Lee J, Shoelson SE. Profilin-1 haploinsufficiency protects against obesity-associated glucose intolerance and preserves adipose tissue immune homeostasis. Diabetes. 2013;62:3718-26.
[9] Elnakish MT, Hassanain HH, Janssen PM. Vascular remodeling-associated hypertension leads to left ventricular hypertrophy and contractile dysfunction in profilin-1 transgenic mice. Journal of cardiovascular pharmacology. 2012;60:544-52.

[10] Adams KE, Ke S, Kwon S, Liang F, Fan Z, Lu Y, et al. Comparison of visible and near-infrared wavelength-excitable fluorescent dyes for molecular imaging of cancer. Journal of biomedical optics. 2007;12:024017.
[11] Kim DE, Kim JY, Schellingerhout D, Shon SM, Jeong SW, Kim EJ, et al. Molecular imaging of cathepsin B proteolytic enzyme activity reflects the inflammatory component of atherosclerotic pathology and can quantitatively demonstrate the antiatherosclerotic therapeutic effects of atorvastatin and glucosamine. Molecular imaging. 2009;8:291-301.
[12] Osborn EA, Jaffer FA. The advancing clinical impact of molecular imaging in CVD. JACC Cardiovascular imaging. 2013;6:1327-41.
[13] Ding Z, Bae YH, Roy P. Molecular insights on context-specific role of profilin-1 in cell migration. Cell adhesion & migration. 2012;6:442-9.
[14] Song B, Jin H, Yu X, Zhang Z, Yu H, Ye J, et al. Angiotensin-converting enzyme 2 attenuates oxidative stress and VSMC proliferation via the JAK2/STAT3/SOCS3 and profilin-1/MAPK signaling pathways. Regulatory peptides. 2013;185:44-51.
[15] Lu T, Wen S, Cui Y, Ju SH, Li KC, Teng GJ. Near-infrared fluorescence imaging of murine atherosclerosis using an oxidized low density lipoprotein-targeted fluorochrome. The international journal of cardiovascular imaging. 2014;30:221-31.
[16] Eckert MA, Vu PQ, Zhang K, Kang D, Ali MM, Xu C, et al. Novel molecular and nanosensors for in vivo sensing. Theranostics. 2013;3:583-94.
[17] Chakravarty R, Goel S, Cai W. Nanobody: the "magic bullet" for molecular imaging? Theranostics. 2014;4:386-98.
[18] Segers FM, den Adel B, Bot I, van der Graaf LM, van der Veer EP, Gonzalez W, et al. Scavenger receptor-AI-targeted iron oxide nanoparticles for in vivo MRI detection of atherosclerotic lesions. Arteriosclerosis, thrombosis, and vascular biology. 2013;33:1812-9.
[19] Bruckman MA, Jiang K, Simpson EJ, Randolph LN, Luyt LG, Yu X, et al. Dual-modal magnetic resonance and fluorescence imaging of atherosclerotic plaques in vivo using VCAM-1 targeted tobacco mosaic virus. Nano letters. 2014;14:1551-8.
[20] Kim WY, Stuber M, Bornert P, Kissinger KV, Manning WJ, Botnar RM. Three-dimensional black-blood cardiac magnetic resonance coronary vessel wall imaging detects positive arterial remodeling in patients with nonsignificant coronary artery disease. Circulation. 2002;106:296-9.
[21] Yeon SB, Sabir A, Clouse M, Martinezclark PO, Peters DC, Hauser TH, et al. Delayed-enhancement cardiovascular magnetic resonance coronary artery wall imaging: comparison with multislice computed tomography and quantitative coronary angiography. Journal of the American College of Cardiology. 2007;50:441-7.
[22] Phinikaridou A, Andia ME, Lacerda S, Lorrio S, Makowski MR, Botnar RM. Molecular MRI of atherosclerosis. Molecules. 2013;18:14042-69.
[23] Chen W, Cormode DP, Vengrenyuk Y, Herranz B, Feig JE, Klink A, et al. Collagen-specific peptide conjugated HDL nanoparticles as MRI contrast agent to evaluate compositional changes in atherosclerotic plaque regression. JACC Cardiovascular imaging. 2013;6:373-84.
[24] Nahrendorf M, Waterman P, Thurber G, Groves K, Rajopadhye M, Panizzi P, et al. Hybrid in vivo FMT-CT imaging of protease activity in atherosclerosis with customized nanosensors. Arteriosclerosis, thrombosis, and vascular biology. 2009;29:1444-51.
[25] Dimastromatteo J, Broisat A, Perret P, Ahmadi M, Boturyn D, Dumy P, et al. In vivo molecular imaging of atherosclerotic lesions in ApoE-/- mice using VCAM-1-specific, 99mTc-labeled peptidic sequences. Journal of nuclear medicine : official publication, Society of Nuclear Medicine. 2013;54:1442-9.